

# A-OctoMap: An Adaptive OctoMap for Online Motion Planning

Yihui Mao<sup>1</sup> and Shuo Liu<sup>1</sup>

**Abstract**—Traditional robotic motion planning methods often struggle with fixed resolutions in dynamically changing environments. To address these challenges, we introduce the A-OctoMap, an adaptive Octo-Tree structure that enhances spatial representation and facilitates real-time, efficient motion planning. This novel framework allows for dynamic space partitioning and multi-resolution queries, significantly improving computational efficiency and precision. Key innovations include a tree-based data structure for enhanced geometric processing, real-time map updating for accurate trajectory planning, and efficient collision detection. Our extensive testing shows superior navigation safety and efficiency in complex settings compared to conventional methods. A-OctoMap sets a new standard for adaptive spatial mapping in autonomous systems, promising significant advancements in navigating unpredictable environments.

## I. INTRODUCTION

### A. Motivation

In the realm of robotics, particularly in motion planning, identifying safe zones in dynamic environments and effectively navigating through complex, narrow settings via optimized control techniques is a critical research area. The ability to swiftly and accurately define safe regions in such dynamic conditions is pivotal for enhancing trajectory planning efficiency and achieving optimal control.

In complex and cluttered environments filled with narrow passages, it becomes especially crucial to implement trajectory planning swiftly while maintaining effective tracking and real-time control over these trajectories (see [1]–[3]).

In the domain of spatial representation, occupancy grid mapping has been a foundational approach due to its straightforward representation of space [4]. However, this method is often limited by its fixed resolution, which constrains adaptability and necessitates a trade-off between detail and storage efficiency.

To address these challenges, we propose a new framework incorporating a novel tree-based data structure for dynamic space partition. This enhancement improves the identification of feasible solutions in congested environments. Our algorithm retains the capability for multi-resolution queries and augments data integration. Utilizing a tree-based data structure, it facilitates multi-threaded geometric processing of localized spatial segments post-partitioning, achieving effective storage and precise representation of spatial data with minimal computational expense. Moreover, our approach ensures the real-time updating of the map in dynamic

environments while preserving critical geometric information, which is vital for dynamic path planning and collision detection.

### B. Related work

1) *Volumetric Representation of Space*: Traditional volumetric reconstruction approaches in robotics have primarily leveraged voxel-based methods, such as voxel-based techniques and hierarchical structures like Octo-Trees [5]. These methods have been favored for their rapid execution, which is crucial for on-the-fly applications in dynamic environments. However, they often fall short when it comes to capturing fine surface details, as they usually sacrifice spatial resolution for computational efficiency.

Despite the speed advantages of voxel-based strategies for 3-D mapping, their lack of granularity often fails in high-fidelity tasks where distinguishing between traversable and obstructed spaces is crucial. Advanced techniques like the Truncated Signed Distance Field (TSDF) and the Euclidean Signed Distance Field (ESDF) offer better distance metrics for motion planning but struggle with data coarseness, limiting resolution and precision in collision avoidance [6], [7]. Additionally, TSDF methods are memory-intensive and computationally challenging to update in real-time for larger environments [8]. In contrast, the emergence of Neural Radiance Fields (NeRF) through deep learning innovations has significantly enhanced autonomous 3-D scene reconstruction, excelling in capturing detailed object surfaces and facilitating sophisticated view planning essential for Simultaneous Localization and Mapping (SLAM) [9], [10]. However, while promising, the computational demands and potential latency in real-time rendering by these neural representation-based methods pose challenges, particularly in dynamic environments requiring high-speed maneuvers.

2) *Point Cloud Downsampling*: The development of point cloud downsampling techniques has primarily focused on balancing efficiency and the preservation of geometric features. Traditional strategies like Farthest Point Sampling (FPS) and Random Sampling (RS) each have their strengths and weaknesses. RS, which involves the random selection of points, is straightforward and fast but fails to preserve geometric features and ensure uniform coverage, resulting in significant information loss [11], [12]. In contrast, FPS iteratively selects the farthest points from those already chosen, ensuring better geometric feature preservation compared to random sampling. However, its computational intensity restricts its use in real-time applications [13].

Voxel-based sampling (VBS) divides space into a grid of voxels and retains a single representative point per voxel,

<sup>1</sup>Y. Mao and S. Liu are with the Department of Mechanical Engineering, Boston University, Brookline, MA, USA. {maoyihui, liushuo}@bu.edu

either the gravity centroid or the original point closest to the centroid. This method offers high computational efficiency suitable for real-time applications and can be combined with RS and FPS strategies, including Uniform Voxel Sampling (UVS) and Voxelized Farthest Points Sampling (VFPS) [14], [15]. However, its fixed voxel size limits adaptability, leading to detail loss in high-density regions, and the use of centroids to represent all points within a voxel results in constant local density.

3-D Edge-Preserving Sampling (3DEPS) has emerged to address these limitations in detail loss [15]. Inspired by sketching techniques, it captures the essence of complex 3-D shapes by emphasizing their sharp edges, providing a more effective representation of intricate objects. 3DEPS utilizes the 3-D Surface Boundary Filter (SBF) to separate the point cloud into edge points and internal points [16]. By adjusting the ratio of these two types of points, a new point cloud is reconstructed, ensuring a balance between preserving edge details and overall point distribution. However, the ratio of edge points to the total number of points is a parameter that must be experimentally tuned, adding complexity to the process.

3) *Path Planning Algorithms*: In motion planning, various methods can be employed to ensure effective collision-free paths. Sampling-based algorithms, such as Rapidly-exploring Random Trees (RRT) and Probabilistic Roadmaps (PRM), achieve impressive results in high-dimensional, complex spaces by randomly expanding searches within the feasible space to find a viable path [17], [18]. The efficiency of these methods heavily relies on the techniques used for sampling points in free regions and the approach to nearest neighbor searches.

Grid search-based algorithms (like Dijkstra, A\*, and their variants) offer resolution completeness ensuring the determination of the shortest path between nodes in grid-based searches. A\*, an extension of the Dijkstra algorithm, utilizes a heuristic approach to estimate the overall path cost, thereby outperforming the Dijkstra algorithm. Jump Point Search (JPS) [19], the optimized algorithm of A\*, was proposed for uniform grids to accelerate search speeds by eliminating certain nodes in the grid based on the setup of jump points. However, all these method are heavily limited by its fixed resolution, which constrains adaptability and necessitates a trade-off between detail and storage efficiency.

### C. Contributions

We propose a novel framework incorporating a novel tree-based data structure to improve the identification of feasible solutions in congested environment. In particular, the contributions are as follows:

- 1) Dynamic space representation: Our dynamic Octo-Tree achieves high-precision segmentation of free spaces and obstacles, effectively addressing the complexities of dynamic environments.
- 2) Spatial representation fidelity: This method supports refined spatial operations and downsampling.

- 3) Efficient collision detection: By parallelizing maximal map polyhedronization and surface triangulation, we achieve efficient collision detection in dynamic environments.
- 4) Integration with navigation methods: This framework accelerates the identification of feasible solutions for grid-based navigation methods (e.g., JPS), thereby enhancing overall navigation efficiency.

## II. PRELIMINARIES

In this section, we introduce some definitions and results on Adaptive OctoMap and Jump Point Search (JPS).

### A. Adaptive OctoMap Node

The attribution of a tree node in the Adaptive OctoMap is present as **Data Structure 1**

---

Data Structure 1: OctreeNode

---

```

1: Struct TreeNode
2: // Common Attributes in vanilla Octotrees
3:   TreeNode* Parent;
4:   TreeNode* Children[2d];
5:   vector<P>PointCloud;
6: // New Attributes in D-octoTree
7:   float SplitBoundry[2d]
8:   float NodeBoundry[2d]
```

---

**Definition 1.** A tree  $T$  can be represented as  $T = (V, E)$  by a set of nodes  $V$  and a set of edges  $E$ :

$$V = \{v_1, v_2, \dots, v_n\}, \quad E = \{(v_i, v_j) \mid v_i, v_j \in V\} \quad (1)$$

Each node  $v_i$  is defined as:

$$v_i = (\text{value}, \text{parent}, \text{children}) \quad (2)$$

where value represents the identifier of Point Cloud, parent represents the parent node ( $\emptyset$  if it is the root), and children represents the set of child nodes.

In this paper, we consider the point cloud as the map storage resource, represented as follows:

$$\mathcal{P} = \{\mathbf{p}_i \mid \mathbf{p}_i \in \mathbb{R}^d, i = 1, 2, \dots, N, d \in \{2, 3\}\} \quad (3)$$

The point cloud  $\mathcal{P}$  is represented as a set containing  $N$  points, where each point  $\mathbf{p}_i$  can be either two-dimensional or three-dimensional.

The attributes **SplitBoundary** and **NodeBoundary** define the boundaries of sub-nodes in an Octree:

- 1) **SplitBoundary**: refers to the boundaries of each sub-node after a node is divided along its axes.
- 2) **NodeBoundary**: represents the actual maximum and minimum values along each axis for the sub-nodes after complete bisection.

---

**Data Structure 2: Octree**

---

- 1: **Struct** OcTree
  - 2: TreeNode\* root;
  - 3: int Depth;
- 

**B. Adaptive OctoMap Tree**

The attribution of a tree in the Adaptive OctoMap is present as **Data Structure 2**:

In this paper, we introduce the concept of Minimum Controllable Region (MCR), which describes the smallest area within which a robot can perform precise control given its control accuracy. This value quantifies the minimal space in which the robot can operate effectively, considering its control precision.

**Definition 2.** The MCR is defined by

$$\text{MCR} = \{ \mathbf{p} \in \mathbb{R}^d \mid \| \mathbf{p} - \mathbf{p}_0 \|_\infty \leq \epsilon_{\max} \}, \quad (4)$$

where  $\mathbf{p} = (x_1, x_2, \dots, x_d)$  is a point in space,  $\mathbf{p}_0 = (x_{0,1}, x_{0,2}, \dots, x_{0,d})$  is the reference point (typically the robot's current position),  $\| \mathbf{p} - \mathbf{p}_0 \|_\infty = \max\{|x_1 - x_{0,1}|, |x_2 - x_{0,2}|, \dots, |x_d - x_{0,d}|\}$  is the *infinity* norm (i.e., the maximum absolute difference in any dimension), and the  $\epsilon_{\max}$  is the estimated upper bound of error.

To determine the depth of a tree, given the exploration range  $L$  along a particular axis (which is determined by the upper bound of the maximum system error  $\epsilon_{\max}$  along the same axis, i.e., the range can be greater than or equal to  $\epsilon_{\max}$ ), we use the following formula:

$$\text{depth} = \left\lceil \log_2 \left( \frac{L}{k \cdot p} \right) \right\rceil, \quad (5)$$

where  $\lceil \cdot \rceil$  denotes the ceiling function, which rounds up to the nearest integer. The  $L$  is the length of the map along a given axis,  $p$  is the size of the MCR along the same axis, and  $k$  is set to a default value (e.g.,  $k = 2$ ), which is a scaling factor to adjust the proportion between the MCR and the node range.

**C. Uniform Grid Map**

The attribution of a uniform grid map is present as **Data Structure 3**

---

**Data Structure 3: uniform grid map**

---

- 1: **Struct** UniformGridMap
  - 2: array <int, d>grid\_map\_amount
  - 3: multi\_array <bool, d>map
- 

**Theorem 1** (Pigeonhole principle). *For natural numbers  $k$  and  $m$ , if  $n = km + 1$  objects are distributed among  $m$  sets, the pigeonhole principle asserts that at least one of the sets will contain at least  $k + 1$  objects [20].*

We conclude that if a grid cell in a uniform grid map has a side length of  $n_s$ , and there exists a gap of at least  $n_s$  meters

within this map, then the boundary of at least one cell must pass through this gap.

**D. Jump Point Search**

A graph search (path planning) algorithm can then be used to identify a valid path that avoids collisions within the grids occupied by obstacles. JPS is suitable for rapid path planning. We define a path, denoted as  $\pi = \langle n_i, \dots, n_j \rangle$ , as a sequence of nodes or states extending from node  $i$  to node  $j$ . The length (or cost) of this path is represented by  $\text{len}(\pi)$ . We introduce the notation  $x$  to refer to a specific node,  $p(x)$  to denote the parent node of  $x$ , and  $\text{neighbours}(x)$  to describe the set of nodes adjacent to  $x$ . Additionally, the node  $n$  is defined as an element within the set of  $\text{neighbours}(x)$ . The expression  $\pi \setminus x$  signifies that node  $x$  is omitted from the path.

In a 2-D map, each node may have up to 8 neighbors. The cost incurred when moving straightly (horizontally or vertically) to a traversable neighbor (not occupied by obstacles) is 1, while moving diagonally has a cost of  $\sqrt{2}$ . For straight moves, if node  $n$  can be reached from  $x$ 's parent  $p(x)$  with the less or equal cost without passing through  $x$ , i.e.,  $\text{len}(\langle p(x), \dots, n \rangle \setminus x) \leq \text{len}(\langle p(x), x, n \rangle)$ , JPS will prune this neighbor  $n$  from exploration. In diagonal moves, the path excluding  $x$  must be strictly shorter,  $\text{len}(\langle p(x), \dots, n \rangle \setminus x) < \text{len}(\langle p(x), x, n \rangle)$ , leading to the pruning of node  $n$ . The natural neighbors of  $x$  are those remaining after pruning, assuming  $\text{neighbours}(x)$  does not include obstacles. Force Neighbors refer to specific neighboring nodes that may not lie directly on the current path but must be examined to ensure the identification of the shortest path, which must satisfy with two conditions. 1)  $n$  is not a natural neighbour 2)  $\text{len}(\langle p(x), x, n \rangle) < \text{len}(\langle p(x), \dots, n \rangle \setminus x)$ . A node qualifies as a jump point if it is either the initial or terminal node, has a forced neighbor, or, in the case of diagonal movement, leads directly to another jump point. as detailed in [19] and [1].

Starting from initial node, the algorithm recursively searches for new jump points in every direction until the terminal node is found or a dead end is reached in that direction. Upon reaching the terminal node, it backtracks through the jump points to construct the shortest path,  $\pi = \langle n_0, n_1, \dots, n_E \rangle$ , from start to finish. Path searching with jump point pruning has been proven to be cost-optimal in [19].

**III. METHODOLOGY****A. Tree build**

We derive the tree depth from Equation (5), ensuring the tree fully covers the entire map. As described in **Algorithm 1** in III-A, the method relies on a multi-level tree structure. This process involves partitioning each level through bisection along different dimensions, ensuring precise allocation of points to their corresponding child nodes. Additionally, each node's boundary is defined by selecting the extremal values (maximum and minimum) in each dimension after the bisection process. These values, along with the node's

boundary, are stored separately in **SplitBoundary** and **NodeBoundary**. The free region within each node can be indirectly represented by these two boundaries at each level. This recursive process is repeated until a leaf node is reached, at which point the current node’s address is pushed into the vector  $\mathcal{L}$ .

---

Algorithm 1: Octree Build

---

```

1: function T. Build( $\mathcal{P}$ )
2: Input:  $\mathcal{P}$ ,  $\mathcal{L}$ 
3: for  $p \in \mathcal{P}$  do
4:   T. push_point_into_tree( $p$ ,  $\mathcal{L}$ )
5: end for

1: function T. push_point_into_tree( $curNode$ ,  $p$ ,  $\mathcal{L}$ )
2: Input:  $p$  // Point
3: OctreeNode  $curNode \leftarrow root$ 
4:  $curNode.depth \leftarrow maxDepth$ 
5: while  $curNode.depth > 0$  do
6:   bisects_each_level_along_axis()
7:    $idx \leftarrow$  allocate and store points to child nodes
8:   if  $curNode.depth == 0$  then
9:      $\mathcal{L}.push\_back(curNode)$ 
10:    return
11:  else
12:    construct_node( $curNode$ ,  $idx$ )
13:     $curNode \leftarrow curNode.children[idx]$ 
14:    push_point_into_tree( $curNode$ ,  $p$ ,  $\mathcal{L}$ )
15:  end if
16: end while

```

---

### B. Uniform Grid Mapping

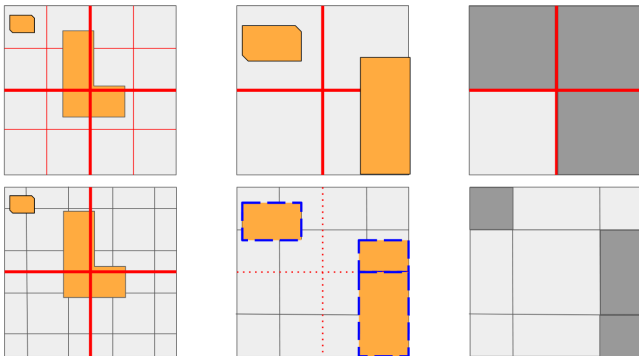


Fig. 1: Illustration of mapping from octree to uniform grid. The top row presents the common method of mapping (Fixed Uniform Grid), while the bottom row presents our method (Adaptive Uniform Grid). The red lines represent the split lines of the octree at one level and its parent level. The blue dotted line represents the node boundary of that node concerning the obstacle on it. The red dotted lines represent the split boundary of that node. The right columns show how the uniform grid would appear based on the two methods.

As shown in Fig. 1, we have developed a novel mapping method that does not solely rely on fixed grid sizes. Instead,

it determines grid occupancy based on obstacle boundaries. The edge length of the uniform grid is equivalent to the MCR edge length. According to Theorem 1, this boundary must intersect the gap and adjust according to the object boundary.

This adjustment is based on the distance between the **SplitBoundary** and the **NodeBoundary**, determining whether a grid should be marked as occupied. In both methods, the edge length of a single uniform grid is equal to half the edge length of the node at the current level. Consequently, this approach does not increase the overall number of grids.

### C. Dynamic Partition

In dynamically changing environments, the limitations of resolution in static uniform grid maps can prevent the guarantee of finding feasible solutions at any given moment. To address this issue, we further subdivide the leaf nodes (see **Algorithm 2**) in III-C until a feasible solution is identified, and store the obstacles in the specific node leaves.

---

Algorithm 2: Dynamic partition

---

```

1: function dynamic_partition( $\mathcal{L}$ )
2: Input:  $\mathcal{L}$  // vector of leaf nodes' address
3: update tree depth
4: for all  $\mathcal{L}$  do
5:    $l \leftarrow \mathcal{L}.pop\_front()$ 
6:   if  $l$  is not nullptr then
7:     for  $p \in \mathcal{P}$  do
8:       push_point_into_tree( $this$ ,  $p$ ,  $\mathcal{L}$ )
9:     end for
10:  end if
11: end for

```

---

### D. Downsampling

In our tree-structured architecture, each child node operates independently, enabling parallel computation for recursive operations and synchronous downsampling of each child node. As shown in **Algorithm 3** in III-D, during the tree construction, the maximum and minimum points in each dimension are determined using the **NodeBoundary**. These external points are used to construct new convex polyhedra at the leaf nodes. By evaluating the positions of the remaining points relative to each extremal face of convex polyhedra, all points within that are eliminated. Points outside the extremal faces are then treated as new candidate extremal points, facilitating construction using quick hull method.

Subsequently, utilizing the Computational Geometry Algorithms Library (CGAL) [21], we apply parallel mesh triangulation to those extreme point in each node to represent the map using meshes. These meshes are then stored within their corresponding nodes, enabling efficient and accurate collision detection.

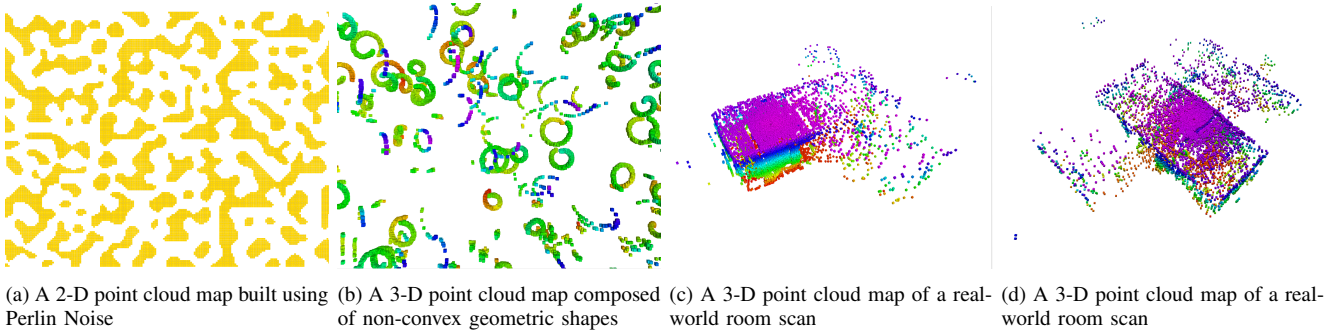


Fig. 2: 4 scenarios used in our experiments to present the efficiency of our method

---

### Algorithm 3: Downsampling

---

```

1: function convexifyPointCloud()
2: Input: branch // branch node
3: convex_vertice // extreme points
4: externalPts  $\leftarrow$  branch.nodeBoundary
5: hex  $\leftarrow$  convex_hull(externalPts)
6: Pts  $\leftarrow$   $\{x \in \text{branch.PointCloud} \mid x \notin \text{HexRegion}\}$ 
7: pts_array  $\leftarrow$  range_search(pts)
8: for  $k \in \{0, \dots, 2^d\}$  do
9: extreme_pts  $\leftarrow$  convex_hull(pts_array[k])
10: convex_vertice.push_back(extreme_pts)
11: end for
12: return convex_vertice

```

---

## IV. COMPLEXITY ANALYSIS AND EXPERIMENTS

### A. Complexity Analysis

Algorithm	Big O Time	Best Case	Worst Case
Tree Build	$O(n \log m)$	$O(n \log m)$	$O(n \log m)$
Uniform Mapping	$O(km)$	$O(k)$	$O(km)$
Dynamic Partition	$O(2^d m)$	$O(2^d)$	$O(2^d \cdot m)$
Downsampling	$O\left(n \log \frac{\hat{n}}{m}\right)$	$O\left(\hat{n} \log \frac{\hat{n}}{m}\right)$	$O\left(\frac{\hat{n}^2}{m}\right)$

TABLE I: Time complexities of different algorithms.

### Notation

- $d$ : The dimension of the map.
- $k$ : The constant value  $k$  in the equation (5)
- $n$ : Total number of points to be mapped.
- $\hat{n}$ : Total number of points after elimination.
- $m$ : Total number of leaf nodes.

In tree building, the time complexity is the same as the original OctoTree build in average and worst cases. Our tree covers the entire map and maintains balance, preventing points from being inserted into a single path to one leaf node. Both the Uniform Mapping and Dynamic Partition are linear algorithms, dependent on the number of leaf nodes.

For downsampling, we store the point cloud in each corresponding leaf node. The best and average cases of the Quickhull method are linearithmic time, while the worst case is quadratic. In our method, points inside the external face are eliminated, resulting in a computation time of  $O\left(\frac{\hat{n}}{m} \log \frac{\hat{n}}{m}\right)$  for each leaf node. The total time complexity is  $O\left(\hat{n} \log \frac{\hat{n}}{m}\right)$  in the best and average cases, and  $O\left(\frac{\hat{n}^2}{m}\right)$  in the worst case.

### B. Experiments

In this section, we present numerical results to demonstrate the effectiveness of our proposed method in four distinct scenarios as shown in Fig. 2, which are based on the RViz in Robot Operation System (ROS) Noetic Ninjemys. We used a Linux desktop with Intel Core i9-13900H running c++ for all computations.

The first scenario is a 2-D map with 35 thousand of point cloud built using Perlin noise, featuring a large number of narrow passages. This setup is designed to test the performance of our algorithm in cluttered environments. The second scenario involves an artificially generated scene

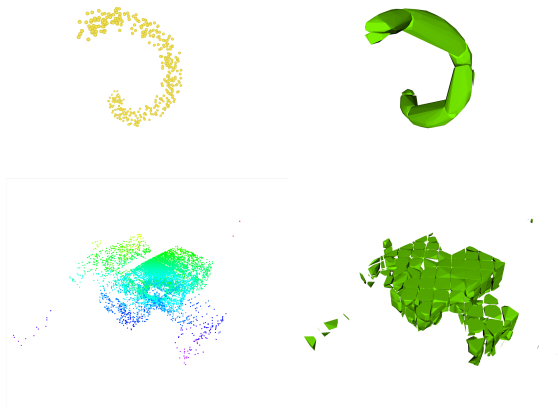


Fig. 3: Illustration of mesh triangulation after downsampling.

Our algorithm accesses the gap areas of each node through the node boundaries, using these areas as minimal bounding boxes to avoid maintaining overall density consistency. Compared to 3D Edge-Preserving Sampling, our method retains the extreme points of the convex hull, enabling local mesh triangulation at a lower computational cost while more effectively preserving critical geometric features. Due to the independence of each node, this approach leverages parallel processing to enhance computational efficiency, making it particularly suitable for real-time applications in robotics and autonomous systems.

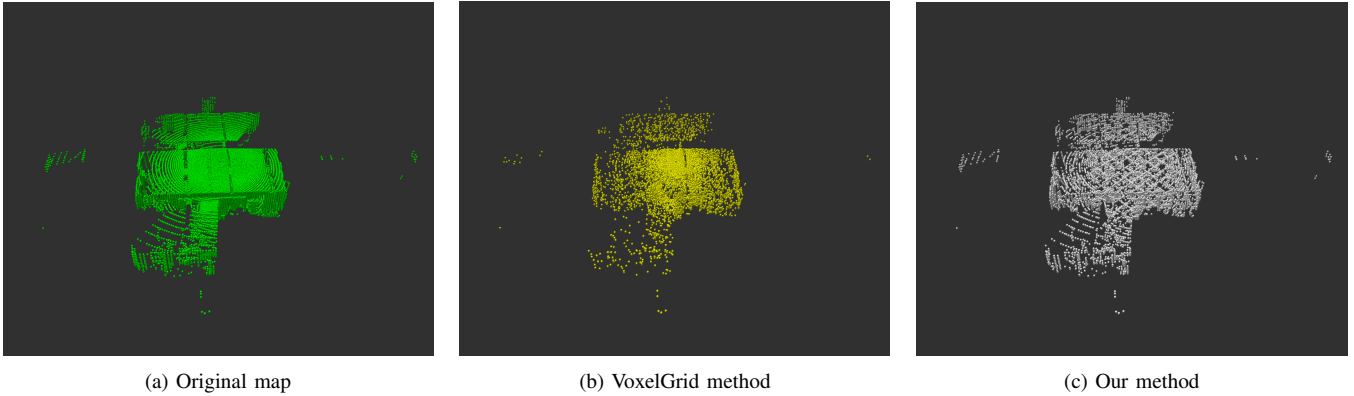


Fig. 4: As shown in the three images above, from left to right: the first image is the original point cloud map, the middle image is the point cloud map processed with a voxel filter, and the third image is our method. Our method preserve critical geometric features.

with non-convex geometric shapes made from point clouds, including arches, helices, cylinders, and cuboids. The third and fourth scenario are based on real-world point cloud maps of rooms, referred to as Room 1 and Room 2, which respectively measures  $30 \times 15 \times 4$  meters and  $26 \times 22 \times 4$  meters, and both contains approximately 110,000 points. These scenarios are used to validate the advanced capabilities of our algorithm through corresponding experiments.

1) *tree build*: The table II shows the performance of tree build in the four scenarios.

Dim	2-D	3-D	3-D	3-D
Scene	Perlin Noise	Geometric Shapes	Room1	Room2
Depth	Time	Time	Time	Time
4	2.47 ms	2.45 ms	4.56 ms	6.68 ms
5	2.56 ms	3.49 ms	5.91 ms	7.57 ms
6	3.71 ms	4.72 ms	7.73 ms	9.01 ms
7	5.04 ms	10.86 ms	11.08 ms	14.41 ms
8	6.73 ms	19.07 ms	26.25 ms	21.17 ms

TABLE II: Time measurements for different levels and scenes.

2) *uniform mapping and dynamic partition*: The table III presents the performance of Uniform Mapping and Dynamic Partition at specific depths of the octo-map. In both Uniform Mapping and Dynamic Partition, the execution times are all in milliseconds, ensuring their viability for online applications.

Algorithm	Uniform Mapping	Dynamic Partition
Depth	Time	Time
4	0.009 ms	1.551 ms
5	0.021 ms	1.566 ms
6	0.044 ms	1.582 ms
7	0.069 ms	1.621ms
8	0.128 ms	1.656 ms

TABLE III: Run time of uniform mapping and dynamic partition.

3) *down sampling and mesh triangulation*: The table IV shows the performance of downsampling and mesh triangulation at the 7th depth of the tree. Observing Table IV,

we can see that the greater the point cloud size, the lower the retention rate (the retention ratio after downsampling). From Fig. 5, it is evident that both the voxel filter and our method retain 10 % of the points from the original map. However, our method retains only the extremal points of the convex hull for each leaf node, which allows us to better preserve the geometric features of the point cloud while discarding redundant points.

Point Cloud Size(k)	Run Time (ms)	Retention Rate (%)
100	41.779	79.23
200	70.806	58.98
300	101.226	48.34
400	115.708	41.48
500	138.764	36.85
600	162.865	34.03
700	181.559	31.86
800	195.756	29.21
900	211.645	27.30

TABLE IV: Run time and retention rate with downsampling.

4) *Jump Point Search*: Figure 5 shows that in the same map, JPS generates paths of different lengths in various types of grid maps. Additionally, in Table V, we tested 1000 different maps generated by Perlin noise. From both Figure 5 and Table V, we can observe that our method has a high probability of finding paths in narrow space environments with shorter path lengths. In all 1000 trials, there was no instance where pathfinding succeeded in the uniform grid but failed with our method.

For rigor, we used Eq. (5) to calculate the tree depth, which allowed us to determine the required number of grids and the grid cell size for my method. We then used a uniform grid of the same cell size for comparison, thus eliminating any size-related advantages. We compared the success rates of feasible solution finding and, in cases where paths were found, the path lengths for both methods across different cell sizes. From the Fig. 6, it is evident that in 1000 maps with dimensions of  $200 \times 150$  meters and approximately 1,200,000 points, there is an overall improvement of at least 6% in the success rate of finding solutions. Additionally, the path length was reduced by more than 6%, and the run time

Cell Size (meter)	Grid Map Dimension	Fixed Uniform Grid	Adaptive Uniform Grid (Our method)	Planning Time
2.6	77×59	683	739	401.63
2.8	73×55	643	721	351.52
3.0	67×51	343	441	301.39
3.2	63×47	177	301	238.8
3.4	59×45	68	128	205.0

TABLE V: JPS feasible solution discovery in 1000 trials and run time (microsecond).

is less than 0.4 ms.

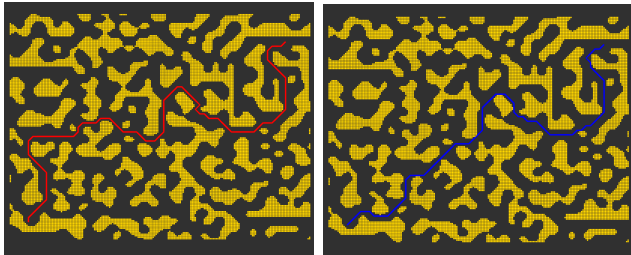


Fig. 5: Illustration of JPS in the map, with dimensions of  $200 \times 150$  meters and approximately 1,200,000 points. The left image (red line path) shows the path finding in the uniform grid map, the right image (blue line path) shows the path finding in the adaptive grid map. The path finding using our method is with shorter path length.

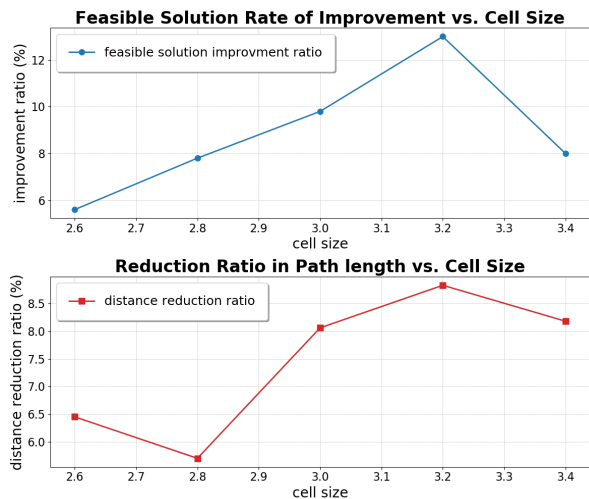


Fig. 6: The feasible solution discovery rate and reduction ratio in path length.

## V. CONCLUSION AND FUTURE WORK

This study has presented a comprehensive framework utilizing an innovative OctoMap structure to enhance spatial representation and dynamic partitioning for efficient motion planning in complex environments. Our approach, underpinned by a novel tree-based data structure, offers high-precision segmentation of free spaces and obstacles, facilitating robust and real-time motion planning capabilities. The framework was validated through rigorous experiments in both simulated and real-world scenarios. These experiments demonstrated the system’s capability to navigate cluttered environments and dynamically adjust to new obstacles, outperforming existing methods in terms of speed and reliability.

Future efforts will be made to scale the solution to larger environments and more diverse scenarios, including outdoor settings with highly unpredictable elements.

## REFERENCES

- [1] S. Liu, M. Watterson, K. Mohta, K. Sun, S. Bhattacharya, C. J. Taylor, and V. Kumar, “Planning dynamically feasible trajectories for quadrotors using safe flight corridors in 3-d complex environments,” *IEEE Robotics and Automation Letters*, vol. 2, no. 3, pp. 1688–1695, 2017.
- [2] S. Liu, J. Zeng, K. Sreenath, and C. A. Belta, “Iterative convex optimization for model predictive control with discrete-time high-order control barrier functions,” in *2023 American Control Conference (ACC)*, 2023, pp. 3368–3375.
- [3] S. Liu and Y. Mao, “Safety-critical planning and control for dynamic obstacle avoidance using control barrier functions,” *arXiv preprint arXiv:2403.19122*, 2024.
- [4] H. Moravec, “Robot spatial perception by stereoscopic vision and 3d evidence grids,” *Perception*, vol. 483, p. 484, 1996.
- [5] A. Hornung, K. M. Wurm, M. Bennewitz, C. Stachniss, and W. Burgard, “Octomap: An efficient probabilistic 3d mapping framework based on octrees,” *Autonomous robots*, vol. 34, pp. 189–206, 2013.
- [6] H. Oleynikova, Z. Taylor, M. Fehr, R. Siegwart, and J. Nieto, “Voxblox: Incremental 3d euclidean signed distance fields for on-board mav planning,” in *2017 IEEE/RSJ International Conference on Intelligent Robots and Systems (IROS)*. IEEE, 2017, pp. 1366–1373.
- [7] L. Han, F. Gao, B. Zhou, and S. Shen, “Fiesta: Fast incremental euclidean distance fields for online motion planning of aerial robots,” in *2019 IEEE/RSJ International Conference on Intelligent Robots and Systems (IROS)*. IEEE, 2019, pp. 4423–4430.
- [8] L. Schmid, M. Pantic, R. Khanna, L. Ott, R. Siegwart, and J. Nieto, “An efficient sampling-based method for online informative path planning in unknown environments,” *IEEE Robotics and Automation Letters*, vol. 5, no. 2, pp. 1500–1507, 2020.
- [9] B. Mildenhall, P. P. Srinivasan, M. Tancik, J. T. Barron, R. Ramamoorthi, and R. Ng, “Nerf: Representing scenes as neural radiance fields for view synthesis,” *Communications of the ACM*, vol. 65, no. 1, pp. 99–106, 2021.
- [10] A. Rosinol, J. J. Leonard, and L. Carlone, “Nerf-slam: Real-time dense monocular slam with neural radiance fields,” in *2023 IEEE/RSJ International Conference on Intelligent Robots and Systems (IROS)*. IEEE, 2023, pp. 3437–3444.
- [11] Y. Eldar, M. Lindenbaum, M. Porat, and Y. Y. Zeevi, “The farthest point strategy for progressive image sampling,” *IEEE transactions on image processing*, vol. 6, no. 9, pp. 1305–1315, 1997.
- [12] C. Moenning and N. A. Dodgson, “Fast marching farthest point sampling,” University of Cambridge, Computer Laboratory, Tech. Rep., 2003.
- [13] J. S. Vitter, “Faster methods for random sampling,” *Communications of the ACM*, vol. 27, no. 7, pp. 703–718, 1984.
- [14] R. B. Rusu and S. Cousins, “3d is here: Point cloud library (pcl),” in *2011 IEEE international conference on robotics and automation*. IEEE, 2011, pp. 1–4.
- [15] D. Li, J. Li, S. Xiang, and A. Pan, “Psegnet: Simultaneous semantic and instance segmentation for point clouds of plants,” *Plant Phenomics*, 2022.
- [16] D. Li, G. Shi, J. Li, Y. Chen, S. Zhang, S. Xiang, and S. Jin, “Plantnet: A dual-function point cloud segmentation network for multiple plant species,” *ISPRS Journal of Photogrammetry and Remote Sensing*, vol. 184, pp. 243–263, 2022.

- [17] S. LaValle, "Rapidly-exploring random trees: A new tool for path planning," *Research Report 9811*, 1998.
- [18] L. E. Kavraki, P. Svestka, J.-C. Latombe, and M. H. Overmars, "Probabilistic roadmaps for path planning in high-dimensional configuration spaces," *IEEE transactions on Robotics and Automation*, vol. 12, no. 4, pp. 566–580, 1996.
- [19] D. Harabor and A. Grastien, "Online graph pruning for pathfinding on grid maps," in *Proceedings of the AAAI conference on artificial intelligence*, vol. 25, no. 1, 2011, pp. 1114–1119.
- [20] Benoît, Rittaud and Heeffer, Albrecht, "The pigeonhole principle, two centuries before Dirichlet," *MATHEMATICAL INTELLIGENCER*, vol. 36, no. 2, pp. 27–29, 2014. [Online]. Available: <http://doi.org/10.1007/s00283-013-9389-1>
- [21] A. Fabri and S. Pion, "Cgal: The computational geometry algorithms library," in *Proceedings of the 17th ACM SIGSPATIAL international conference on advances in geographic information systems*, 2009, pp. 538–539.